THE JOURNAL OF PHYSICAL CHEMISTRY LETTERS
A JOURNAL OF THE AMERICAN CHEMICAL SOCIETY

pubs.acs.org/JPCL

Letter

Dependence between Structural and Electronic Properties of $CsPbI_3$: Unsupervised Machine Learning of Nonadiabatic Molecular Dynamics

Spencer M. Mangan, Guoqing Zhou, Weibin Chu, and Oleg V. Prezhdo*

Cite This: *J. Phys. Chem. Lett.* 2021, 12, 8672–8678

Read Online

ACCESS | Metrics & More | Article Recommendations | Supporting Information

ABSTRACT: Using unsupervised machine learning on the trajectories from a nonadiabatic molecular dynamics simulation with time-dependent Kohn–Sham density functional theory, we elucidated the structural parameters with the largest influence on nonradiative recombination of charge carriers in $CsPbI_3$, which forms the basis for solar energy and optoelectronic applications. The I–I–I angles between PbI_6 octahedra, followed by the Cs–I distance, have the strongest impact on the bandgap and the nonadiabatic coupling. The importance of the Cs–I distance is unexpected, because Cs does not contribute to electron and hole wave functions. The nonadiabatic coupling is most influenced by static properties, which is also surprising, given its explicit dependence on atomic velocities.

Inorganic halide perovskites are a promising class of electronic materials with many potential applications, including photovoltaics, electronic displays, nanocrystals, and light-emitting devices.[1] Compared to hybrid organic–inorganic perovskites, they exhibit better material stability and charge carrier behavior more amenable to devices.[2] Metal halide perovskites in general have been a popular topic of research over the past decade with an extremely diverse set of potential applications.[3−8] However, the charge carrier dynamics which govern the performance of perovskites in electronic devices are quite complicated and not fully understood.[9] While many studies have focused on the geometric and electronic structures of the perovskite crystals, theoretical investigations of their charge carrier dynamics are rare because of the high computational cost of simulation and the difficulty of computing properties such as the nonadiabatic coupling (NAC).[10−13] Despite these limitations, simulation remains a promising method for understanding the quantum dynamics of perovskite solar cells. Analysis of the quantum dynamics simulations requires an understanding of the correlations of the key electronic properties, such as excitation energies and NACs, with the material's geometric features.

Nonadiabatic molecular dynamics (NA-MD) for atomic motions combined with time-dependent density functional theory (TD-DFT) for electronic evolution is the gold standard for modeling systems with coupled electronic and nuclear degrees of freedom.[11,12,14−17] It requires no *a priori* knowledge of the mechanism of the process simulated and avoids the approximations inherent to phenomenological theories. TD-DFT allows for the relatively low-cost calculation of excited-state energies and NACs compared to other methodologies, enabling the large-scale application of NA-MD toward materials simulation.[18] The resulting information from combining NA-MD with TD-DFT is similar to what would result from time-resolved pump–probe spectroscopy measurements.[19]

Machine learning (ML) has found many scientific applications in recent years; it can be an extremely powerful tool in data analysis and has been used to great effect in many research fields.[20−23] ML can be especially useful when dealing with noisy data because of its ability to find correlations that are otherwise difficult to predict, such as those which are nonlinear. Careful application of ML can be used on systems such as lead halide perovskites in order to extract information that is otherwise nearly impossible to predict and can even cut through noise.[24]

ML can be either supervised or unsupervised. In supervised learning a labeled output is used to learn or approximate relationships between input and observed output.[25] Unsupervised learning has no labeled output and is used to infer hidden structures and similarities in a data set. As demonstrated in previous work,[24] unsupervised ML can generate valuable

Received: July 21, 2021
Accepted: August 27, 2021
Published: September 2, 2021

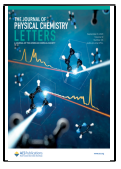

https://doi.org/10.1021/acs.jpclett.1c02361
J. Phys. Chem. Lett. 2021, 12, 8672–8678

insights into the charge carrier dynamics of halide perovskites. The trajectories from a NA-MD simulation can be analyzed to extract features, such as crystalline angles, atomic distances, and the nuclear velocity, and unsupervised ML can then be used on the features and the electronic properties to hunt for correlations that would not otherwise be immediately legible.

In this Letter, we apply ML to analyze the Hamiltonian of the real-time TD-DFT and NA-MD simulation of charge carrier dynamics in $CsPbI_3$, an inorganic halide perovskite considered promising for solar cell applications. We demonstrate the main influence on the charge carrier properties of the material to be the angles of the lead−iodine backbone and the distance between the cesium and iodine atoms. We also demonstrate the importance of static geometry over atomic motion. Both of these results are unexpected and could not be guessed *a priori*, because the NAC is calculated from the atomic velocity, and cesium atoms do not contribute to electron and hole wave functions.

The study was performed on β-$CsPbI_3$,[26,27] which was represented by a $\sqrt{2} \times \sqrt{2} \times 2$ unit cell with lattice constants of 9.05 Å × 9.05 Å × 12.94 Å. The simulation was performed with the Vienna Ab Initio Simulation Package (VASP) using the PBE exchange−correlation functional and projector-augmented wave method. The Brillouin zone was sampled with a 4 × 4 × 2 Monkhorst−Pack k-point mesh. The structure was optimized and then thermalized at room temperature, and a 7 ps microcanonical trajectory was obtained with a 1 fs time step. The 7 ps trajectory was sufficient to sample the motions present in the system. The NAC

$$\begin{aligned}\mathbf{d}_{ji} &= -\mathrm{i}\hbar\langle\varphi_j(\mathbf{r}, \mathbf{R}(t))|\nabla_{\mathbf{R}}|\varphi_i(\mathbf{r}, \mathbf{R}(t))\rangle\frac{\mathrm{d}\mathbf{R}}{\mathrm{d}t}\\ &= -\mathrm{i}\hbar\frac{\langle\varphi_j(\mathbf{r}, \mathbf{R}(t))|\nabla_{\mathbf{R}}H(\mathbf{R}(t))|\varphi_i(\mathbf{r}, \mathbf{R}(t))\rangle}{E_i - E_j}\frac{\mathrm{d}\mathbf{R}}{\mathrm{d}t}\\ &= -\mathrm{i}\hbar\left\langle\varphi_j(\mathbf{r}, \mathbf{R}(t))\left|\frac{\partial}{\partial t}\right|\varphi_i(\mathbf{r}, \mathbf{R}(t))\right\rangle\\ &\approx -\frac{\mathrm{i}\hbar}{2\Delta t}\{\langle\varphi_j(\mathbf{r}, \mathbf{R}(t))|\varphi_i(\mathbf{r}, \mathbf{R}(t + \Delta t))\rangle\\ &\quad - \langle\varphi_j(\mathbf{r}, \mathbf{R}(t + \Delta t))|\varphi_i(\mathbf{r}, \mathbf{R}(t))\rangle\}\end{aligned} \tag{1}$$

was calculated via the Python extension for ab initio dynamics (PYXAID),[11,12] a methodology with a substantial track record of agreement with experiment.[14−16,28−41] The phase consistency of the NAC was considered explicitly.[42−44] The three most important features influencing perovskite charge carrier dynamics are generally the bandgap, the NAC, and the coherence time between pairs of states. The coherence time is a function of the bandgap. Thus, our methodology extracts information about the bandgap and the NAC to test for correlations between charge carrier dynamics and structural features.[45]

Once the simulation was complete, various geometric features, such as bond distances and angles between atoms, were extracted into a time series for each feature. There was a total of 162 such geometric features in the cell. Unsupervised ML was then used to compare the time evolution of each of these 162 geometric features to that of the 2 electronic properties. Both the bandgap and the NAC were correlated to both the geometric features and their time derivatives, leading to a total of 324 features. Visualization of the crystal structures and features were created in part with VESTA.[46]

Because of the highly nonlinear nature of the correlations in play, mutual information (MI) offers an attractive way to quantify the relationship between the structural and electronic behaviors of the crystal. In units of information (bits, nats, etc.), the mutual information quantifies the shared dependence of two variables, specifically the amount of information contained about the other variable in one. Because it describes the correlation in terms of information instead of lines or polynomials, it is a much better choice than methods such as Pearson correlation. It ranges from 0 to ∞ for no shared information to two identical variables.

The pairwise MI, $I(X, Y)$, between each feature and the bandgap or the NAC was calculated via k-nearest neighbor statistics,[47,48] with $k = 3$, which has previously been demonstrated to give the best results with halide perovskites.[24]

$$I(X, Y) = \iint \mathrm{d}x\,\mathrm{d}y\,p(x, y)\log_2\left(\frac{p(x, y)}{p(x)p(y)}\right) \tag{2}$$

where $p(x, y)$ is the joint probability density function of the two variables and $p(x)$ and $p(y)$ are the marginal probability density functions. The individual features were then averaged for each type for comparison and analysis. In other words, each I−I−I angle present in the system has its own mutual information. The MI for all I−I−I angles was averaged to create the MI value for I−I−I, and so on for each type of feature.

Figure 1 displays the ideal geometric structure of $CsPbI_3$, along with several of the features considered in the present

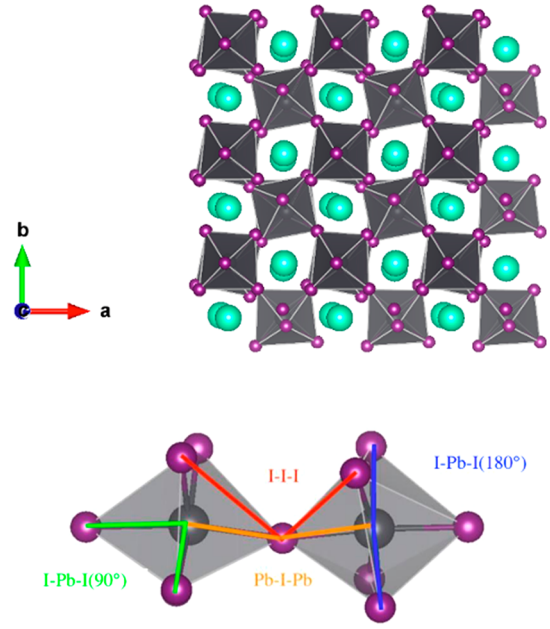

Figure 1. Geometric structure of $CsPbI_3$ and the feature angles.

study. The Cs^+ cation occupies the A-site of the generic ABX_3 structure of metal halide perovskites and is free to move within its cage of lead and iodine atoms, and the relatively open space in the cell allows for significant movement. The Cs^+ ion exhibits a "rattling" behavior between two different sites in the lattice.[49]

Figure 2 displays the time evolution of the bandgap and the NAC of the simulated $CsPbI_3$ perovskite. The bandgap falls within the energy range of solar photons, which makes $CsPbI_3$

https://doi.org/10.1021/acs.jpclett.1c02361
J. Phys. Chem. Lett. 2021, 12, 8672−8678

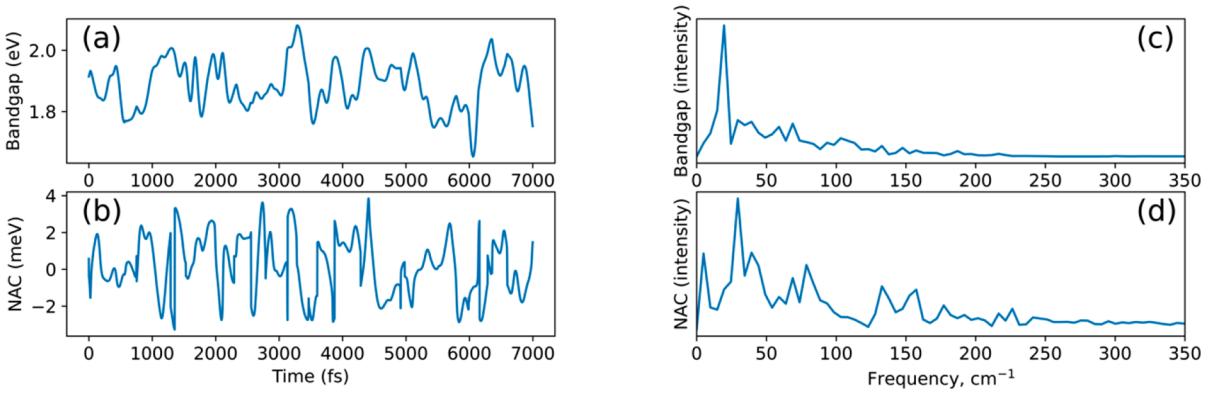

Figure 2. Time evolution of (a) bandgap and (b) NAC between the CBM and the VBM of pristine $CsPbI_3$, as well as Fourier transforms of the same (c) bandgap and (d) NAC. The NAC exhibits a broader range of frequencies than the bandgap.

a promising material for solar cells.[2] The valence band maximum (VBM) of lead iodide perovskites arises from atomic orbitals of lead and iodine atoms, while the conduction band minimum (CBM) is formed by atomic orbitals of lead. The Fourier transforms (FTs) of the bandgap and NAC evolutions demonstrate that the NAC fluctuates over a broader range of frequencies, including higher frequencies, compared to the bandgap. This is because the NAC is a more complex electronic property than the bandgap. It is more sensitive to spatial distribution of electron and hole wave functions and depends explicitly on atomic velocity (eq 1).

Tables 1 and 2 present the results for the MI (eq 2) of the five most important features with the bandgap and the NAC.

Table 1. Mutual Information with Standard Deviation (SD) of Bandgap with Features of $CsPbI_3$ Crystal

feature	MI ± SD (bits)
I−I−I angle	2.71 ± 0.08
Cs−I distance	2.47 ± 0.18
Pb−I−Pb angle	2.38 ± 0.14
I−Pb−I (∼90°) angle	2.36 ± 0.09
Cs−I motion	2.33 ± 0.10

Table 2. Mutual Information with Standard Deviation (SD) of NAC with Features of $CsPbI_3$ Crystal

feature	MI ± SD (bits)
I−I−I angle	2.59 ± 0.04
Cs−I distance	2.39 ± 0.20
I−Pb−I (∼90°) angle	2.27 ± 0.08
Pb−I−Pb angle	2.26 ± 0.13
Cs−I motion	2.23 ± 0.13

The standard deviations (SD) are computed from the distribution of the MI values for each feature of a given type. For example, considering the two most important features, there are 9 distinct I−I−I angles and 33 distinct Cs−I distances (Table S1), and the SD are computed from the distributions of 9 and 33 MI values, respectively. The MI for the bandgap is slightly larger than for the NAC because the bandgap exhibits better correlation with the features than the NAC. The NAC is a more complex function of system geometry, and its relationship to particular structural features and motions is weaker than for the bandgap.

The results are quite unusual. First, both the bandgap and the NAC share substantial mutual information with the Cs−I distance and its motion. Cs atoms do not contribute to either the VBM or the CBM, and therefore, Cs atoms should not influence the bandgap and the NAC between these states. The influence of Cs atoms on the electronic properties of the VBM and the CBM arises through short-range steric interactions of Cs with iodine atoms, as well as through long-range electrostatic interactions of the Cs^+ cation with the electron and the hole.

Second, the NAC correlates much more strongly with geometries than motions, even though the NAC depends explicitly on the atomic velocity (eq 1). Again, surprisingly, the Cs−I bond plays an important role. Its motion correlates with the NAC more than, for example, the motion of the Pb−I bond or motion of any of the angles involving I and Pb atoms.

Third, the bandgap correlates with the Cs−I motion as much as the NAC does. This is unexpected, because the bandgap depends only on atomic positions. The correlation of the bandgap with the atomic velocities can be explained by the fact that the velocity is a time-derivative of the geometry, and thus, a geometric feature and its velocity share information. In other words, the velocity is correlated to the geometry just as the bandgap is, which causes the Cs−I motion to share some information with the bandgap.

Fourth, it is unexpected that the top 5 features correlated with the bandgap and the NAC are identical. The rest of the features can be found in Tables S2 and S3 of the Supporting Information. Although the NAC is inversely proportional to the energy gap (eq 1), it depends strongly on localization of the VBM and CBM wave functions. The present system contains no defects. The VBM and the CBM are delocalized over the whole system and change little as the system fluctuates around its equilibrium geometry. One can expect larger differences between the most important features influencing the bandgap and the NAC in systems containing defects,[19] or at higher temperatures that result in increased structural disorder and partial charge localization.[50]

Fifth, the preeminent influence of the I−I−I angle on the perovskite's electronic properties is also somewhat surprising. Its MI with both the bandgap and the NAC is notably larger than that of any other feature (Tables 1 and 2). The importance of the PbI_6 geometry is expected because of the aforementioned localization of the VBM and the CBM to the lead and iodine atoms. Therefore, the high rank of the angles formed by the I and Pb atoms is not surprising. However, previous literature[51,52] argues that the formation of polarons and the magnitude of the bandgap are governed by the Pb−I−

https://doi.org/10.1021/acs.jpclett.1c02361
J. Phys. Chem. Lett. 2021, 12, 8672−8678

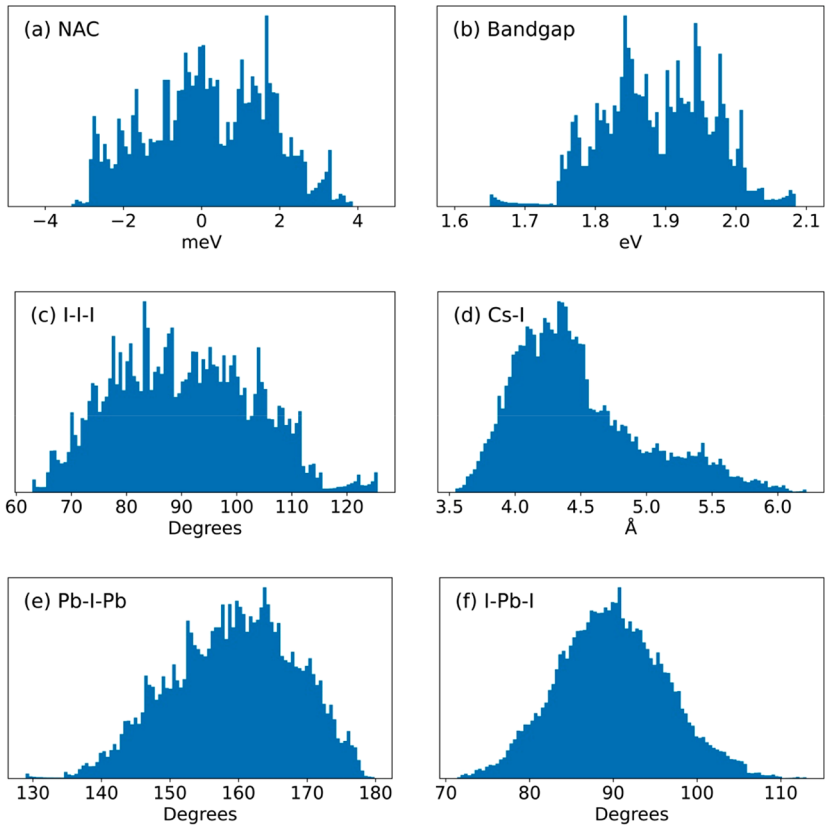

Figure 3. Probability distributions of (a) NAC; (b) bandgap; (c) I−I−I, (e) Pb−I−Pb, and (f) I−Pb−I angles; and (d) Cs−I distance. These features have the highest mutual information with the NAC and bandgap.

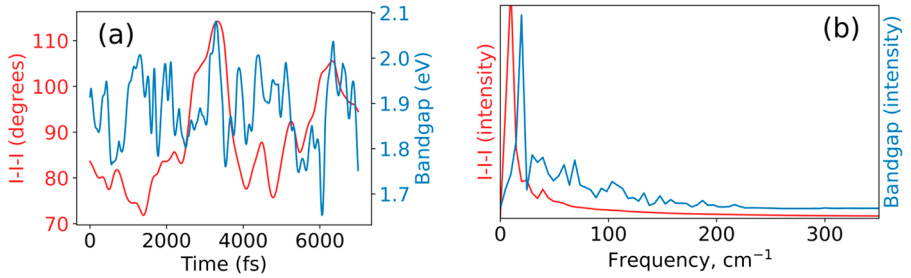

Figure 4. (a) Example of an individual feature plotted against the bandgap and (b) their Fourier transforms.

Pb angle, which is important in our analysis, but ranks notably lower than the I−I−I angle. Both I−I−I and Pb−I−Pb angles measure the tilt between PbI_6 octahedra, a fact which continues to support the importance of octahedral tilt in determining charge carrier behavior. Of the other important factors, the ∼90° I−Pb−I angle describes deformation within the octahedron.

The hybrid organic−inorganic analogue, $MAPbI_3$ with MA = CH_3NH_3, of the all inorganic $CsPbI_3$ perovskite exhibits some, but not all of these unusual correlations.[24] In particular, the coordinates or motions of the organic MA^+ cation are ranked lower for both the bandgap and the NAC, compared to the coordinates and motions of the Cs^+ cation. The much lighter MA^+ species carries weaker influence on the inorganic Pb−I lattice composed of heavy elements. One can conclude in general that the mass mismatch decouples the organic and inorganic components of hybrid perovskites. The stronger influence of atomic geometry than atomic motion on the bandgap and the NAC is seen in both all-inorganic $CsPbI_3$ and hybrid organic−inorganic $MAPbI_3$ perovskite. The fact that the same features correlate most with the bandgap and the NAC holds for both types of materials. The highest MI associated with the I−I−I angle is independent of the nature of the A-site cation as well.

Figure 3 gives a visualization of the distributions of the NAC, bandgap, and several geometric features most highly correlated to them. It is worth noting the very small magnitude of the NAC, which is roughly three orders of magnitude smaller than the bandgap. The NAC can be important despite its small value: as governed by Fermi's golden rule, the recombination rate is proportional to the square of the NAC; hence, its variance can have significant effects.[53] The Pb−I−Pb angles, which have a substantial effect on polaron formation, are distributed around roughly 165° instead of 180°.[51,54]

Figure 4a presents superimposed time evolutions of a single, most significant feature and the bandgap. The feature, the I−I−I angle, is most strongly correlated with the bandgap, with the pairwise mutual information $I(X, Y)$ = 2.77 bits (Table 1).

https://doi.org/10.1021/acs.jpclett.1c02361
J. Phys. Chem. Lett. 2021, 12, 8672−8678

It is hard to discern any correlation between the feature and the bandgap from the time-series representation. After FTs are taken (Figure 4b), the relation becomes somewhat clearer; the large spike in the bandgap intensity is twice the frequency of the large spike of the I−I−I intensity. This demonstrates the benefits of using MI, because a simpler method, such as Pearson correlation, would not be able to establish a relationship from these graphs.

A similar methodology with MI was applied by Zhou et al. to the $MAPbI_3$ perovskite, finding a similar role in I−I−I distortions and static PbI_6 geometry, but with otherwise divergent results that benefit from explanation.[24] The main finding of that research is corroborated by the current study, namely, that the I−I−I is the main structural factor governing the electronic properties in lead halide perovskites. However, in this work, the cation's involvement is substantially different in both nature and degree.

The high MI between the Cs−I distance and the bandgap in $CsPbI_3$ does not have an analogue in $MAPbI_3$ for either the MA^+ cation or the individual ion's coordinates. Given that the VBM and CBM are localized on the Pb−I lattice, the influence of the Cs^+ and MA^+ cations on the electron and hole properties can proceed either via long-range electrostatic interactions or indirectly via cation-induced deformations of the PbI_6 octahedra. Both cations carry the same charge, while MA^+ has a more complex and less symmetrical charge distribution. Therefore, one can expect that MA^+ should have a stronger electrostatic influence on the properties of the charges. For example, MA^+ rotations can lead to charge localization,[55] while Cs^+ rotations can have no such effect. Because Cs exhibits stronger correlations with the bandgap and the NAC than MA,[24] spatial repulsive interactions is the dominant effect. The greater amount of shared information observed by our study corroborates results that observe Cs^+ ions have a stronger distortional effect on the Pb−I backbone than do MA^+ or FA^+ ions in the analogous perovskite crystals.[54] Figure 5 displays relevant parts of the structure for the all-inorganic and hybrid organic−inorganic perovskites.

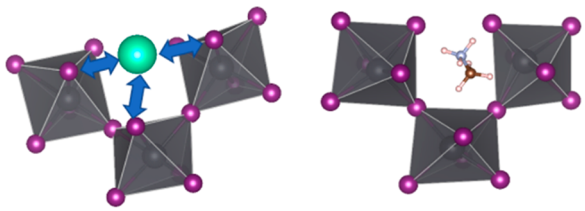

Figure 5. Positioning of the Cs^+ (left) and MA^+ (right) cations within the Pb−I lattice.

The other difference between the all-inorganic $CsPbI_3$ vs the hybrid organic−inorganic $MAPbI_3$ is in the range of the MI values for the bandgap and the NAC (Tables 1 and 2). The bandgap and NAC MI values are similar for $CsPbI_3$, while they differ by a factor of three for $MAPbI_3$.[24] The bandgap MI values are of the same order for $CsPbI_3$ and $MAPbI_3$; however, the NAC MI values are three times smaller for $MAPbI_3$. It is hard to find a straightforward rationalization for this difference, because proper normalization of MI is not easy to achieve (see section S3 of the Supporting Information). Likely, it is the result of the dependence of the NAC on atomic motions. The smaller number of atoms in the $CsPbI_3$ simulation cell, compared to $MAPbI_3$, leads to the higher correlation. The greater influence of the Cs^+ ions on the NAC, compared to the MA^+ ions, further increases the MI between the features and the NAC.

In summary, by applying unsupervised ML to analyze correlations between structural and electronic properties of the $CsPbI_3$ perovskite, we have established the key geometric features and motions that govern charge carrier dynamics in this popular solar cell material. We have demonstrated a number of unusual results that could not have been found without the use of ML. Unexpectedly, both the location and motion of Cs^+ cations play important roles, ranking number 2 and 5, respectively. This is surprising, because the charges are supported by the Pb and I atoms of the inorganic lattice, and Cs atoms have no contribution to the electron and hole wave functions near the band edges. The positions and motions of the corresponding MA^+ cation in the hybrid organic−inorganic $MAPbI_3$ perovskite are less important. The indirect influence of Cs^+ and MA^+ on the charge carrier dynamics can occur either via long-range electrostatic interaction with the charges or by steric repulsion with the Pb−I lattice. The fact that the heavier and more symmetrical Cs^+ carries a stronger influence than the lighter MA^+ with an asymmetric charge distribution indicates that the steric interaction is more important. The mass mismatch decouples the organic and inorganic components in $MAPbI_3$, while the heavy Cs^+ ion strongly couples to the Pb−I lattice. Also unexpectedly, structure is more important for the NAC than geometry, even though the NAC is directly proportional to atomic velocity. Here, the length and velocity of Cs−I bonds have higher ranks than the length and velocity of Pb−I bonds. The bandgap and the NAC correlate with the same features, including both geometries and motions, even though the bandgap is determined solely by geometry. The most important feature is the I−I−I angle, with the Pb−I−Pb octahedral tilt angle having the third most important role after the I−I−I angle and the Cs−I bond. For those interested in engineering the properties of $CsPbI_3$ and related materials, we confirm the high importance of the PbI_6 tilt geometry. The fact that the I−I−I angle and the Cs−I bond are the most important structural properties indicates that changing and mixing halogen atoms can be used to control and optimize charge carrier dynamics in metal halide perovskites.

■ ASSOCIATED CONTENT

Supporting Information

The Supporting Information is available free of charge at https://pubs.acs.org/doi/10.1021/acs.jpclett.1c02361.

Theoretical details and complete mutual information tables (PDF)

■ AUTHOR INFORMATION

Corresponding Author

Oleg V. Prezhdo − *Department of Physics and Astronomy and Department of Chemistry, University of Southern California, Los Angeles, California 90089, United States;* orcid.org/0000-0002-5140-7500; Email: prezhdo@usc.edu

Authors

Spencer M. Mangan − *Mork Family Department of Chemical Engineering and Materials Science, University of Southern California, Los Angeles, California 90089, United States*

https://doi.org/10.1021/acs.jpclett.1c02361
J. Phys. Chem. Lett. 2021, 12, 8672−8678

Guoqing Zhou − *Department of Physics and Astronomy, University of Southern California, Los Angeles, California 90089, United States;* orcid.org/0000-0002-4000-8467
Weibin Chu − *Department of Chemistry, University of Southern California, Los Angeles, California 90089, United States;* orcid.org/0000-0001-5951-0337

Complete contact information is available at: https://pubs.acs.org/10.1021/acs.jpclett.1c02361

Notes

The authors declare no competing financial interest.

■ ACKNOWLEDGMENTS

This work was supported by U.S. National Science Foundation Grant No. CHE-1900510.

■ REFERENCES

(1) Kovalenko, M. V.; Protesescu, L.; Bodnarchuk, M. I. Properties and Potential Optoelectronic Applications of Lead Halide Perovskite Nanocrystals. *Science* **2017**, *358* (6364), 745−750.
(2) Deng, J.; Li, J.; Yang, Z.; Wang, M. All-Inorganic Lead Halide Perovskites: A Promising Choice for Photovoltaics and Detectors. *J. Mater. Chem. C* **2019**, *7*, 12415−12440.
(3) Rong, Y.; Hu, Y.; Mei, A.; Tan, H.; Saidaminov, M. I.; Seok, S. I.; McGehee, M. D.; Sargent, E. H.; Han, H. Challenges for Commercializing Perovskite Solar Cells. *Science* **2018**, *361*, eaat8235.
(4) Xing, G.; Mathews, N.; Sun, S.; Lim, S. S.; Lam, Y. M.; Gratzel, M.; Mhaisalkar, S.; Sum, T. C. Long-Range Balanced Electron- and Hole-Transport Lengths in Organic-Inorganic $CH_3NH_3PbI_3$. *Science* **2013**, *342*, 344−347.
(5) Green, M. A.; Ho-Baillie, A. Perovskite Solar Cells: The Birth of a New Era in Photovoltaics. *ACS Energy Lett.* **2017**, *2*, 822−830.
(6) Manser, J. S.; Christians, J. A.; Kamat, P. V. Intriguing Optoelectronic Properties of Metal Halide Perovskites. *Chem. Rev.* **2016**, *116*, 12956−13008.
(7) Brenner, T. M.; Egger, D. A.; Kronik, L.; Hodes, G.; Cahen, D. Hybrid Organic—Inorganic Perovskites: Low-Cost Semiconductors with Intriguing Charge-Transport Properties. *Nat. Rev. Mater.* **2016**, *1*, 15007.
(8) Herz, L. M. Charge-Carrier Mobilities in Metal Halide Perovskites: Fundamental Mechanisms and Limits. *ACS Energy Lett.* **2017**, *2*, 1539−1548.
(9) Ghosh, D.; Welch, E.; Neukirch, A. J.; Zakhidov, A.; Tretiak, S. Polarons in Halide Perovskites: A Perspective. *J. Phys. Chem. Lett.* **2020**, *11*, 3271−3286.
(10) Craig, C. F.; Duncan, W. R.; Prezhdo, O. V. Trajectory Surface Hopping in the Time-Dependent Kohn-Sham Approach for Electron-Nuclear Dynamics. *Phys. Rev. Lett.* **2005**, *95*, 163001.
(11) Akimov, A. V.; Prezhdo, O. V. The PYXAID Program for Non-Adiabatic Molecular Dynamics in Condensed Matter Systems. *J. Chem. Theory Comput.* **2013**, *9*, 4959−4972.
(12) Akimov, A. V.; Prezhdo, O. V. Advanced Capabilities of the PYXAID Program: Integration Schemes, Decoherence Effects, Multiexcitonic States, and Field-Matter Interaction. *J. Chem. Theory Comput.* **2014**, *10*, 789−804.
(13) Wang, L.; Akimov, A.; Prezhdo, O. V. Recent Progress in Surface Hopping: 2011−2015. *J. Phys. Chem. Lett.* **2016**, *7*, 2100−2112.
(14) Prezhdo, O. V. Multiple Excitons and the Electron−Phonon Bottleneck in Semiconductor Quantum Dots: An Ab Initio Perspective. *Chem. Phys. Lett.* **2008**, *460*, 1−9.
(15) Wang, L.; Long, R.; Prezhdo, O. V. Time-Domain Ab Initio Modeling of Photoinduced Dynamics at Nanoscale Interfaces. *Annu. Rev. Phys. Chem.* **2015**, *66*, 549−579.
(16) Long, R.; Prezhdo, O. V.; Fang, W. Nonadiabatic Charge Dynamics in Novel Solar Cell Materials. *Wiley Interdiscip. Rev.: Comput. Mol. Sci.* **2017**, *7*, e1305.
(17) Li, W.; She, Y.; Vasenko, A. S.; Prezhdo, O. V. *Ab Initio* Nonadiabatic Molecular Dynamics of Charge Carriers in Metal Halide Perovskites. *Nanoscale* **2021**, *13*, 10239−10265.
(18) Tapavicza, E.; Bellchambers, G. D.; Vincent, J. C.; Furche, F. Ab Initio Non-Adiabatic Molecular Dynamics. *Phys. Chem. Chem. Phys.* **2013**, *15*, 18336.
(19) Li, W.; Long, R.; Tang, J.; Prezhdo, O. V. Influence of Defects on Excited-State Dynamics in Lead Halide Perovskites: Time-Domain Ab Initio Studies. *J. Phys. Chem. Lett.* **2019**, *10*, 3788−3804.
(20) Lo, Y.-C.; Rensi, S. E.; Torng, W.; Altman, R. B. Machine Learning in Chemoinformatics and Drug Discovery. *Drug Discovery Today* **2018**, *23*, 1538−1546.
(21) Bertone, G.; Deisenroth, M. P.; Kim, J. S.; Liem, S.; Austri, R. R. de; Welling, M. Accelerating the BSM Interpretation of LHC Data with Machine Learning. *Phys. Dark Universe* **2019**, *24*, 100293.
(22) Yu, Y.; Tan, X.; Ning, S.; Wu, Y. Machine Learning for Understanding Compatibility of Organic−Inorganic Hybrid Perovskites with Post-Treatment Amines. *ACS Energy Lett.* **2019**, *4*, 397−404.
(23) Butler, K. T.; Davies, D. W.; Cartwright, H.; Isayev, O.; Walsh, A. Machine Learning for Molecular and Materials Science. *Nature* **2018**, *559*, 547−555.
(24) Zhou, G.; Chu, W.; Prezhdo, O. V. Structural Deformation Controls Charge Losses in $MAPbI_3$: Unsupervised Machine Learning of Nonadiabatic Molecular Dynamics. *ACS Energy Lett.* **2020**, *5*, 1930−1938.
(25) Wang, B.; Chu, W.; Tkatchenko, A.; Prezhdo, O. V. Interpolating Nonadiabatic Molecular Dynamics Hamiltonian with Artificial Neural Networks. *J. Phys. Chem. Lett.* **2021**, *12*, 6070−6077.
(26) Wang, Y.; Dar, M. I.; Ono, L. K.; Zhang, T.; Kan, M.; Li, Y.; Zhang, L.; Wang, X.; Yang, Y.; Gao, X.; et al. Thermodynamically Stabilized β-$CsPbI_3$-Based Perovskite Solar Cells with Efficiencies > 18%. *Science* **2019**, *365*, 591−595.
(27) Chu, W.; Saidi, W. A.; Zhao, J.; Prezhdo, O. V. Soft Lattice and Defect Covalency Rationalize Tolerance of B-$CsPbI_3$ Perovskite Solar Cells to Native Defects. *Angew. Chem., Int. Ed.* **2020**, *59*, 6435−6441.
(28) Zhang, L.; Vasenko, A. S.; Zhao, J.; Prezhdo, O. V. Mono-Elemental Properties of 2D Black Phosphorus Ensure Extended Charge Carrier Lifetimes under Oxidation: Time-Domain Ab Initio Analysis. *J. Phys. Chem. Lett.* **2019**, *10*, 1083−1091.
(29) Li, L.; Long, R.; Bertolini, T.; Prezhdo, O. V. Sulfur Adatom and Vacancy Accelerate Charge Recombination in MoS_2 but by Different Mechanisms: Time-Domain Ab Initio Analysis. *Nano Lett.* **2017**, *17*, 7962−7967.
(30) Zhang, Z.; Liu, L.; Fang, W.-H.; Long, R.; Tokina, M. V.; Prezhdo, O. V. Plasmon-Mediated Electron Injection from Au Nanorods into MoS_2: Traditional versus Photoexcitation Mechanism. *Chem.* **2018**, *4*, 1112−1127.
(31) Long, R.; Casanova, D.; Fang, W.-H.; Prezhdo, O. V. Donor−Acceptor Interaction Determines the Mechanism of Photoinduced Electron Injection from Graphene Quantum Dots into TiO_2: π-Stacking Supersedes Covalent Bonding. *J. Am. Chem. Soc.* **2017**, *139*, 2619−2629.
(32) Chaban, V. V.; Prezhdo, V. V.; Prezhdo, O. V. Covalent Linking Greatly Enhances Photoinduced Electron Transfer in Fullerene-Quantum Dot Nanocomposites: Time-Domain Ab Initio Study. *J. Phys. Chem. Lett.* **2013**, *4*, 1−6.
(33) Lu, T.-F.; Wang, Y.-S.; Tomko, J. A.; Hopkins, P. E.; Zhang, H.-X.; Prezhdo, O. V. Control of Charge Carrier Dynamics in Plasmonic Au Films by TiO_X Substrate Stoichiometry. *J. Phys. Chem. Lett.* **2020**, *11*, 1419−1427.
(34) Yang, Y.; Fang, W.-H.; Benderskii, A.; Long, R.; Prezhdo, O. V. Strain Controls Charge Carrier Lifetimes in Monolayer WSe_2: Ab Initio Time Domain Analysis. *J. Phys. Chem. Lett.* **2019**, *10*, 7732−7739.
(35) Long, R.; Prezhdo, O. V. Asymmetry in the Electron and Hole Transfer at a Polymer−Carbon Nanotube Heterojunction. *Nano Lett.* **2014**, *14*, 3335−3341.

(36) Long, R.; English, N. J.; Prezhdo, O. V. Defects Are Needed for Fast Photo-Induced Electron Transfer from a Nanocrystal to a Molecule: Time-Domain *Ab Initio* Analysis. *J. Am. Chem. Soc.* **2013**, *135*, 18892−18900.
(37) Long, R.; English, N. J.; Prezhdo, O. V. Minimizing Electron−Hole Recombination on TiO_2 Sensitized with PbSe Quantum Dots: Time-Domain Ab Initio Analysis. *J. Phys. Chem. Lett.* **2014**, *5*, 2941−2946.
(38) Cheng, C.; Fang, W.-H.; Long, R.; Prezhdo, O. V. Water Splitting with a Single-Atom Cu/TiO_2 Photocatalyst: Atomistic Origin of High Efficiency and Proposed Enhancement by Spin Selection. *JACS Au* **2021**, *1*, 550−559.
(39) Sarkar, R.; Kar, M.; Habib, M.; Zhou, G.; Frauenheim, T.; Sarkar, P.; Pal, S.; Prezhdo, O. V. Common Defects Accelerate Charge Separation and Reduce Recombination in CNT/Molecule Composites: Atomistic Quantum Dynamics. *J. Am. Chem. Soc.* **2021**, *143*, 6649−6656.
(40) Wang, Z.; Altmann, P.; Gadermaier, C.; Yang, Y.; Li, W.; Ghirardini, L.; Trovatello, C.; Finazzi, M.; Duò, L.; Celebrano, M.; et al. Phonon-Mediated Interlayer Charge Separation and Recombination in a $MoSe_2/WSe_2$ Heterostructure. *Nano Lett.* **2021**, *21*, 2165−2173.
(41) Zhou, G.; Lu, G.; Prezhdo, O. V. Modeling Auger Processes with Nonadiabatic Molecular Dynamics. *Nano Lett.* **2021**, *21*, 756−761.
(42) Chu, W.; Zheng, Q.; Akimov, A. V.; Zhao, J.; Saidi, W. A.; Prezhdo, O. V. Accurate Computation of Nonadiabatic Coupling with Projector Augmented-Wave Pseudopotentials. *J. Phys. Chem. Lett.* **2020**, *11*, 10073−10080.
(43) Chu, W.; Prezhdo, O. V. Concentric Approximation for Fast and Accurate Numerical Evaluation of Nonadiabatic Coupling with Projector Augmented-Wave Pseudopotentials. *J. Phys. Chem. Lett.* **2021**, *12*, 3082−3089.
(44) Akimov, A. V. A Simple Phase Correction Makes a Big Difference in Nonadiabatic Molecular Dynamics. *J. Phys. Chem. Lett.* **2018**, *9*, 6096−6102.
(45) Akimov, A. V.; Prezhdo, O. V. Persistent Electronic Coherence Despite Rapid Loss of Electron−Nuclear Correlation. *J. Phys. Chem. Lett.* **2013**, *4*, 3857−3864.
(46) Momma, K.; Izumi, F. *VESTA 3* for Three-Dimensional Visualization of Crystal, Volumetric and Morphology Data. *J. Appl. Crystallogr.* **2011**, *44*, 1272−1276.
(47) Kraskov, A.; Stögbauer, H.; Grassberger, P. Estimating Mutual Information. *Phys. Rev. E* **2004**, *69*, 066138.
(48) Khan, S.; Bandyopadhyay, S.; Ganguly, A. R.; Saigal, S.; Erickson, D. J.; Protopopescu, V.; Ostrouchov, G. Relative Performance of Mutual Information Estimation Methods for Quantifying the Dependence among Short and Noisy Data. *Phys. Rev. E* **2007**, *76*, 026209.
(49) Straus, D. B.; Guo, S.; Abeykoon, A. M.; Cava, R. J. Understanding the Instability of the Halide Perovskite $CsPbI_3$ through Temperature-Dependent Structural Analysis. *Adv. Mater.* **2020**, *32*, 2001069.
(50) Li, W.; Tang, J.; Casanova, D.; Prezhdo, O. V. Time-Domain Ab Initio Analysis Rationalizes the Unusual Temperature Dependence of Charge Carrier Relaxation in Lead Halide Perovskite. *ACS Energy Lett.* **2018**, *3*, 2713−2720.
(51) Miyata, K.; Meggiolaro, D.; Trinh, M. T.; Joshi, P. P.; Mosconi, E.; Jones, S. C.; De Angelis, F.; Zhu, X.-Y. Large Polarons in Lead Halide Perovskites. *Sci. Adv.* **2017**, *3*, e1701217.
(52) Filip, M. R.; Eperon, G. E.; Snaith, H. J.; Giustino, F. Steric Engineering of Metal-Halide Perovskites with Tunable Optical Band Gaps. *Nat. Commun.* **2014**, *5*, 5757.
(53) Hyeon-Deuk, K.; Madrid, A. B.; Prezhdo, O. V. Symmetric Band Structures and Asymmetric Ultrafast Electron and Hole Relaxations in Silicon and Germanium Quantum Dots: Time-Domain Ab Initio Simulation. *Dalton Trans.* **2009**, *45*, 10069−10077.
(54) Mahata, A.; Meggiolaro, D.; De Angelis, F. From Large to Small Polarons in Lead, Tin, and Mixed Lead−Tin Halide Perovskites. *J. Phys. Chem. Lett.* **2019**, *10*, 1790−1798.
(55) Zhang, Z.; Long, R.; Tokina, M. V.; Prezhdo, O. V. Interplay between Localized and Free Charge Carriers Can Explain Hot Fluorescence in the $CH_3NH_3PbBr_3$ Perovskite: Time-Domain Ab Initio Analysis. *J. Am. Chem. Soc.* **2017**, *139*, 17327−17333.

https://doi.org/10.1021/acs.jpclett.1c02361
J. Phys. Chem. Lett. 2021, 12, 8672−8678